7 Experimental Methods of Optical Spectroscopy

7.1 Methods Involving Thermic Radiation

Dispersive spectral photometers with monochromators and Fourier instruments that can capture absorption over a large frequency range both operate with thermal radiation sources. The emitter should be as "white" a source as possible, i. e. it should have a homogenous distribution of the radiant intensity in the spectral range under study. The best possible conditions are achieved by black body radiators, see chapter 2.4. Infrared glowers have temperatures between 500 K and 1800 K. The Nernst glower is a small ceramic tube of yttrium and zirconium oxide, that at a temperature of 1800 K produces the spectrum of a black body. It needs to be heated initially, because its conductivity is poor at room temperature, and it has a short lighting time. A glow bar is made of silicon carbide (SiC), conducts at room temperature, and produces the spectrum of a black body at 1400 K. At 500 K, the emission maximum is at $\lambda = 5$ µm. Nickel-chrome filaments are also used. It is, however, unavoidable (see chapter 2.4), that in the mid IR range from 4000 cm^{-1} to 400 cm^{-1} the radiant energy is reduced by approximately three orders of magnitude. In the far infrared, mercury high pressure lamps are used below 100 cm^{-1}. The plasma in the cylinders and the red glowing silicate cylinders emit. In the near infrared and in the visible range, halogen lamps with a filament of tungsten are used. In the UV range, deuterium lamps are common.

It is possible to transmit though gas, liquid, and thin solid samples. Powders are compressed into thin leaves, in which a powdered alkali halogenide powder can be used as an IR transparent bonding agent. Thick solid body samples of low tranmittivity are measured by reflection or scattering. For rough surfaces, light radiation can be alternated between measurement and control samples in a diffuse-reflection measurement with photometer spheres. Through the spherical geometry, as much scattered light as possible is reflected onto the detector. For smooth surfaces, an attenuated total reflectance setup (ATR) can be used. This takes advantage of the low penetration of the light rays totally reflected on the walls of a medium which is transparent to IR and has a relatively large index of refraction into the neighboring (to be studied) medium.
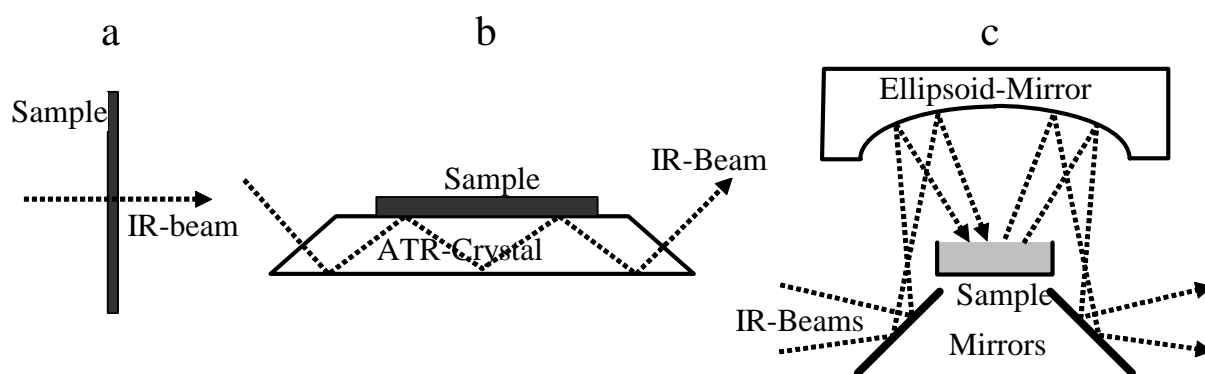

Fig. 7.1 Arrangement of the samples for transmission (a), ATR (b), and diffuse reflexion (c).

The time resolution (upper cutoff frequency) of the detectors should be higher than the sampling rate of the measurement setup. As we will see, the sampling rate corresponds to the rotation frequency of the mirror in dispersive double-beam spectrometers and to the reciprocal time delay between two measurement steps in a Fourier spectrometer, which is registered by the analog-to-digital converter when the mirror is shifted. Thermal radiation detectors achieve sampling rates between 10 and 1000 Hz. A good time resolution is achieved when the IR light is focused (with a KBr lens) onto a vacuum thermocouple. Golay cells can achieve a maximum of 100 Hz. Here the warping of a mirror caused by the expansion of a noble gas is seen in the image of a ruled grating. Bolometers have been using the effect that the electric resistance of materials depends on temperature for more than 100 years. Modern bolometers use semiconductors, e.g. small helium cooled silicon crystals, and achieve cutoff frequencies in the kHz range and also low thermal noise in the detector as compared to the noise of the light source. Pyroelectric detectors, e.g. predeuterated triglycine sulfate (DTGS) make use of the strong temperature dependence of the polarization just below their Curie temperature and achieve high cutoff frequencies though with reciprocally diminishing sensitivity. Semiconductor materials in which light quanta raise the electrons from the valence band into the conduction band (photovoltaics) are called quantum detectors. Different detectors have optimal sensitivity over limited ranges of the light spectrum. In the UV/VIS range, photomultiplier tubes (PMT's) are used as radiation detectors. This range also profits from the developments in digital photography: linear arrangements of photodiodes with a diode separation of about 100 µm (*photo diode array,* PDA) measure the light of different wavelengths behind the dispersive portion (lattice) simultaneously and achieve thereby much higher detection sensitivity than individual measurements with a PMT. In CCD's (*charge coupled device*), the incoming photo energy is saved as a charge in a metal oxide semiconductor (MOS). The stored charge is amplified by the semiconductor component and electronically measured.

7.1.1 *Dispersive Double-Beam Spectral Photometers*

Until the establishment of Fourier transform infrared spectrometers around 1980, dispersive spectrometers were used for the entire optical spectral range. Now they are only used in the UV/VIS range. *Two* channel methods directly produce a difference spectrum of a sample to a comparison material (e. g. the solvent in liquid samples) and thus produce a measured spectrum independent of many disturbances caused by the measuring device, e. g. variations in the amplification of electronic components. In the two-beam alternating light method, the measurement beam and the control beam were sent to a monochromator alternately by a segment mirror rotating with a frequency of about 10 Hz. After the optical detector, narrow band low frequency amplification (e.g. 10±1 Hz) and phase sensitive detection (with a lock in amplifier) is done with the reference voltage source, which also rotates the mirror with a synchronous motor. The output of the rectifier controls the optical attenuation of the reference beam (comb shaped diaphragm in the beam path), which is coupled with the plot of the transparency of the sample. The plot of the wavelength scale is coupled with the position of the monochromator. Couplings used to be mechanical, now they are electronically controlled.
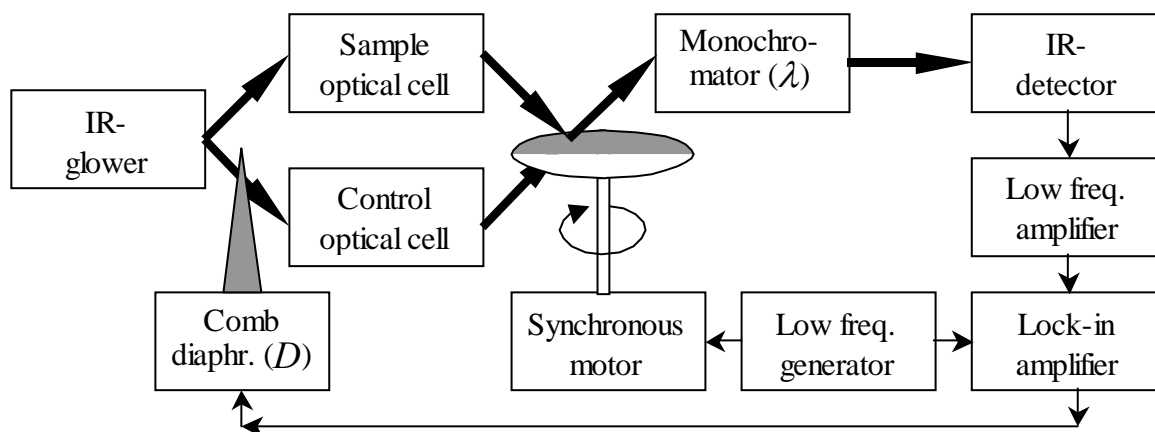
Fig. 7.2 Design of a dispersive automatically aligning double-beam spectral photometer.
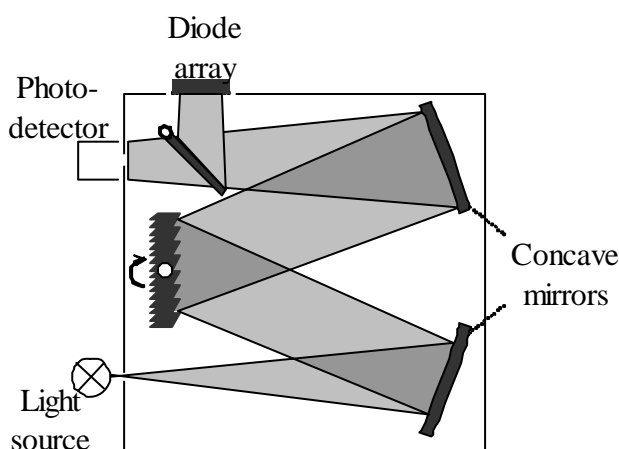

Fig. 7.3 Monochromator with reversible grating and output for a diode array.

Monochromators are the dispersive elements of a spectrometer. They image a narrow frequency range of the light at the entrance slit onto the output slit. (*slit width* from 10 µm to 1 mm, larger for array detectors). The light outside this range is lost. The frequency range is shifted by changing the angle of a prism or grating. Criteria for the performance of the monochromator are, on the one hand, transmission and light-gathering power, and on the other hand the resolving power. Glass and quartz block transmittion in the middle and far IR; quartz is transparent in the near IR. For this reason, alkali-halogenide single crystals are used as the material for prisms and lenses in the middle IR range. The more transparent this material is in the infrared frequency range, the poorer the resolving power becomes. LiF has high dispersion, but is only transparent up to $1800\ cm^{-1}$. CsJ is transparent up to $200\ cm^{-1}$, but has much lower dispersion.

After initial use of alkali-halogenide single crystals, diffraction gratings on a plane or concave (generally reflective) surface are used as the dispersive element since about 1960. They have a high resolving power but reduced light-gathering power due to the distribution of the intensity over many orders. To optimize the resolving power, the groove distance should be approximately equal to the wavelength. Therefore multiple changeable gratings are used one spectrometer that covers a larger wavelengths range. Higher orders of diffraction have higher resolution but lower intensity and a smaller frequency interval. To concentrate the light intensity on the smallest number of orders, the grooves are given a certain blaze angle. In a monochromator, two gratings can be used in series, or one can be used multiple times with a mirror.
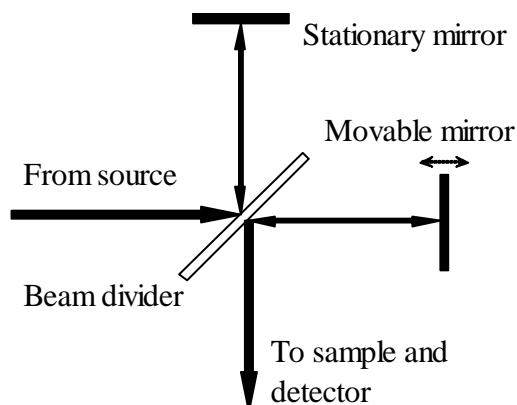
7.1.2 Fourier Spectrometers

Fig. 7.4 Michelson interferometer

Optical FT spectrometers do not have monochromators but rather interferometers, typically a Michelson interferometer with a movable mirror (1-30 mm s^{-1}). The information is in a time domain acquired by recording the signal in steps at whole number multiples of a selected difference of the optical path. This signal in the time domain has to be transformed into the frequency domain through a Fourier transformation, which used to be a disadvantage only at the beginning of Fourier spectroscopy around 1970, but not now.

An important advantage over dispersive spectrometers gives the two orders of magnitude higher light-gathering power due to the larger opening (aperture stop, AS) from the lack of a narrow entrance slit. The second and most significant advantage as compared to a normal monochromator (without a detector array) comes from the fact that the luminous intensity over the whole frequency domain is being continuously processed by the receiver. This is in contrast to a monochromator, where only a narrow frequency range is detected, determined by the resolution $\Delta \nu$ (smallest frequency difference of separable signals). This is referred to as the *multiplex advantage* and improves the signal to noise ratio in a simultaneously detected spectral range $\nu_{Max} - \nu_{Min}$ by the root of M, where M is defined by $\nu_{Max} - \nu_{Min} = M \Delta \nu$. A third advantage is the high accuracy of the frequency calibration through the use of a guide laser (usually a helium-neon laser, which is red at 633 nm). The laser beam running through the interferometer creates, on a separate detection channel, a pure sinus function whose zero points are used as a trigger for the analogue-to-digital converter in the signal channel. The mirror must be in motion at a constant velocity. A second phase-shifted detector and detection channel allows quadrature detection, which makes it possible to differentiate between forward and backward motion of the mirror. This in turn allows exact placement of the recorded signals (at zero-point passage) to positive and negative difference path lengths in signal accumulation through multiple back and forth motions of the mirror.

The intensity (energy density) of a beam is proportional to the square of the electric field strength. In chapter 2, equ.(2.01), it was shown that the electric field strength can be described by a function of the form

$$E = A \cos(k_x x - 2\pi \nu t), \tag{7.01}$$

where x is the direction of propagation. For the wave number we have $k_x = 2\pi/\lambda$. Let us now consider at which frequency an interference maximum is shifted when the optical path difference (which is reflected over the movable and stationary mirrors) of both beams is changed by $\Delta x = 2 \nu t$ through motion of the mirror at speed ν. An overlapping of the field strengths of both beams leads to an addition of the functions (for the same amplitude A)

$$\cos(k_x x - 2\pi \nu t) + \cos(k_x [x + \Delta x] - 2\pi \nu t). \tag{7.02}$$

In the construction of the square of the field strength, we then get

$$\cos^2(k_x x - 2\pi\nu t) + \cos^2(k_x[x + \Delta x] - 2\pi\nu t) + 2\cos(k_x x - 2\pi\nu t)\cos(k_x[x + \Delta x]) - 2\pi\nu t). \quad (7.03)$$

For the last term we can use the addition theorem $2\cos(\alpha)\cos(\beta) = \cos(\alpha + \beta) + \cos(\alpha - \beta)$. From that we get in the sum:

$$\cos^2(k_x x - 2\pi\nu t) + \cos^2(k_x[x + \Delta x] - 2\pi\nu t) + \cos(k_x[2x + \Delta x] - 4\pi\nu t) + \cos(k_x[-\Delta x]) \quad (7.04)$$

The first three terms are functions of ν, which, when averaged over exactly one or infinit many optical oscillation periods have the numerical value of one. The final term $\cos(k_x[-\Delta x])$ can be written as $\cos(k_x 2\nu t)$. It contains the phase difference multiplied by the wave number, which propagates at the speed 2ν. This phase speed is the speed of the propagation of the maximum of the two interfering wave trains. The phase speed of light in a vacuum is c_0. With that, the frequency of an observed oscillation is reduced by the factor $2\nu/c_0$, when $\nu = 15$ mm s^{-1} thus approximately by the factor 10^{-10}. The helium-neon laser frequency is reduced from $4{,}74 \times 10^{14}$ Hz in optical observation to 47,4 kHz in the interferogram with a mirror speed of 15 mm s^{-1}. All frequencies of infrared are transformed by the interferometer into the low frequency range and are thus readily accessible to electronics. Also, the zero passes of the interferogram of the laser supply a sufficiently rapid trigger for the entire infrared range.

The sampling theory named after Harry Nyquist tells us that for the unique identification of a cosine function, at least two measurements must be taken per oscillation period. For the duration of the sampling of a measurement value (dwell time) τ we then get $\tau < 1/(2\nu)$ or in other words, the sampling rate has to be at least twice the oscillation frequency to be measured. If the sampling rate is exactly double or less, we get, after Fourier transformation, mirror symmetric replicates or aliasing. These are mirrored into the unique spectral range from $1/(2\tau)$ from outside. If the sampling rate is much higher than twice the frequency of the sampled signal, no advantage is gained in non-noisy signals. This so-called oversampling, however, simplifies the determination of signals buried in noise.

Time between sampling (dwell time): $\Delta t = 1$ ms

Fig. 7.5 Measurements with a dwell time of 1 ms. The dashed line with a frequency of 250 Hz has 4 measured values per period (double oversampling). The dotted 500 Hz line contains only 2 measured values per period and, after a Fourier transformation, would appear on both edges of the frequency range from 0 to 500 Hz, since it is indiscernible from 0 Hz (all points pass through a line). The 1 kHz line contains only one measured point per period and would be mirrored in to both edges of the measurement range.

Frequency domain of the Fourier transformation:

0 Hz   250 Hz   500 Hz
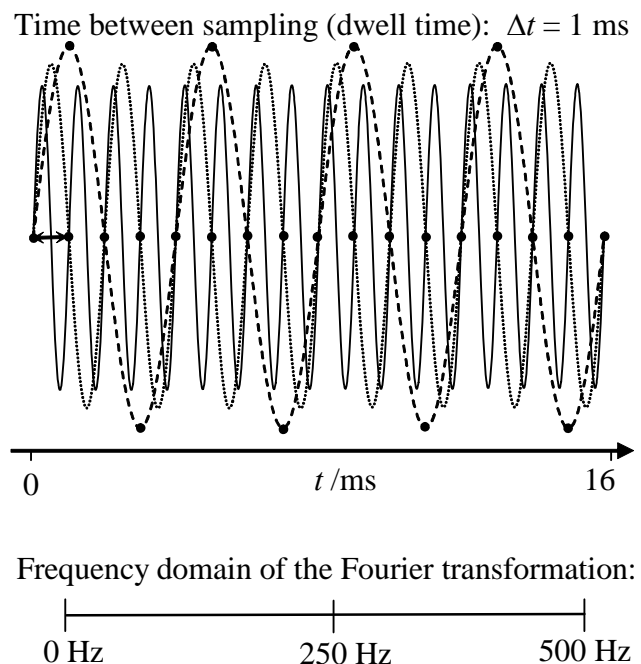
The interferogram (intensity as a function of the difference path length) of a sample does not represent a cosine function, unlike the interferogram of a laser beam. The Fourier Transformation of the cosine function is a delta function (infinitely thin and infinitely high, integral over the function is one). Also the overlapping of two pure frequencies, which produce beats, has no practical use. The experimentally observed spectra with finite line widths produce interferograms, which can be described as damped cosine functions, see Fig 7.6.
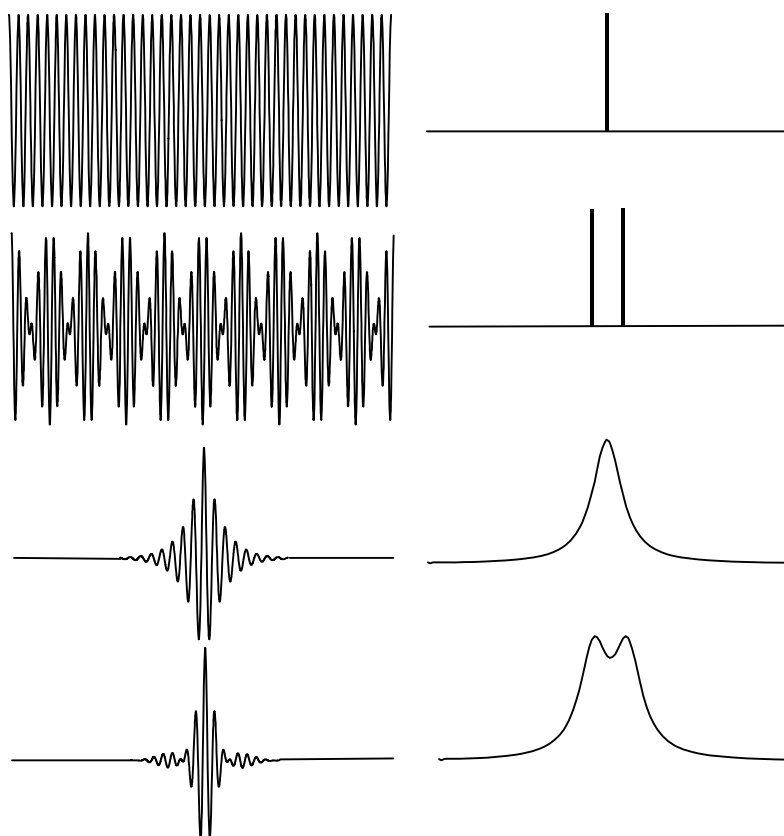

Fig. 7.6 Interferograms (left) and spectra (right). The two upper curves show pure cosine functions (which are continued infinitely to the left and right) and their Fourier transformations (delta functions). Here the two frequencies of the second curve have a deviation of ± 10 % from the frequency of the first curve. The two lower curves are real interferograms and are similar to absorption curves. Their average frequencies are exactly analogous to those of the upper curves. The interferograms fall to zero symmetrically with the difference wavelengths.

7.1.3   *Notes about Luminescence, Fluorescence and Phosphorescence*

Apart from lasers, we distinguish between thermal radiators and luminescent radiators. The latter is the emission of light after an energy absorption occurs, which *is not* caused by heating.The light absorbed usually has higher energy than the light later emitted. There is photoluminescence, electroluminescence (through injection, electron collision, or field ionization), cathode luminescence (picture tubes), chemoluminescence, bioluminescence, etc. Fluorescence (first observed by George Gabriel Stokes in CaF_2) and phosphorescence (weakly glowing phosphorous demonstrates this phenomenon caused by lattice imperfections) divide luminescence into quickly ($< 10^{-8}$ s) and slowly subsiding phenomena. The separation can also be made with respect to monomolecular or bimolecular phenomena, or according to the dying out of the intensity, i.e. if the dying out follows an exponential function or hyperbolic function. A sharp distinction between the two terms does not exist. For this reason it was recommended (to no avail) that in the optical domain we should only speak about luminescence. In the X-ray range, fluorescence is the term of choice.

7.2   Laser

Lasers (Light Amplification by Stimulated Emission of Radiation) exist since 1960, when Theodore Harold Maiman built the first ruby laser, which produced a deep red light. Today, lasers produce light in the UV, visible, IR and up to the 3 mm microwave range (for Masers, which were built a few years before the first laser). Lasers can produce continuous power ranging from μW to 100 kW. Power burst reach TW. Focusing the beam of a 100 W cw (continuous wave) laser onto 10 μm^2 produces a radiation density of 10 TW m^{-2}.

Lasers as spectroscopic radiation sources have much higher monochromatic radiant power than thermal radiators and can thus improve the sensitivity of cw spectrometers. Semiconductor lasers of the Pb row cover the IR range from 4000 cm^{-1} to 400 cm^{-1} in multiple intervals from 50-200 cm^{-1} with a resolution of 10^{-4} cm^{-1}. Raman spectrometers have lower demands on the frequency variation. Completely new spectroscopic methods are sprouting from the use of short laser pulses, with which time resolved optical spectroscopy in the picosecond range can be done. See chapter 7.3.

7.2.1   Operating Conditions

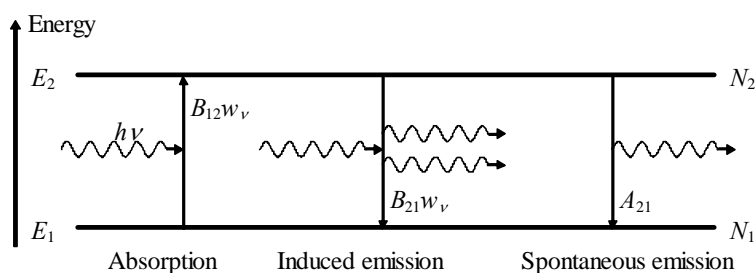*First operating condition:* the induced emission must be greater than the absorption.

Fig. 7.7 Spontaneous and induced emission (identical to Fig. 2.3)

In the notation introduced in chapter 2, this condition is defined $N_2B_{21}w_\nu > N_1B_{12}w_\nu$. If, for the sake of simplicity, we set the weighting factors of the two states $g_1 = g_2$ (as in chapter two by excluding different degeneracies of the two states) then, $B_{21} = B_{12}$ and from $N_2B_{21}w_\nu > N_1B_{12}w_\nu$ it follow for the first lasing condition that:

$$N_2 > N_1. \tag{7.05}$$

In thermal equilibrium it still holds from the validity of the Boltzmann statistics that $N_2 < N_1$. Thus we see the necessity of a population inversion.

Such an inversion is reached (discussed in detail below) by

> ➢ Optical pumping,
> ➢ collision excitation,
> ➢ excitation with an electric current or,
> ➢ chemical processes.

Oscillation excitation is achieved by back coupling. This method for creating oscillations from electronics couples a selected frequency from the amplifier output with the same phase to the amplifier input. The positive feedback coupling in lasers is attained by attaching two mirrors which are concave or plane-parallel and perpendicular to the z axis of the system.
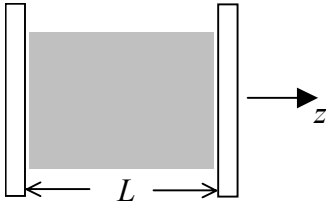

Fig. 7.8 A Fabry-Pérot-resonator composed of two widely separated mirrors in the x-z-plane, with the medium in the middle.

The noise intensity created in the resonator by spontaneous emission is amplified for one frequency by multiple reflections from the mirrors in the active medium if the resonator length L is a multiple of the corresponding wavelength and the medium contains transitions of this frequency with $N_2 < N_1$. The mirror on the left has a reflectivity of almost 100 %. Only a very small part of the intensity exits from the mirror on the right, which has a reflectivity < 100 %. The cooperation of resonator and active medium leads to sharp frequencies, directional bundles, and high spectral energy density.

Another operating condition is identical to the *oscillation condition* in electronics and can be expressed by

$$\text{amplification} > \text{damping} \qquad \text{or} \qquad \text{gain} > \text{losses.} \tag{7.06}$$

At the beginning of an oscillation, the occupation numbers of the levels are assumed constant. It holds that

$$dI = \sigma I (N_1 - N_2)\, dz = -\alpha I\, dz, \tag{7.07}$$

where I is the photon number flux density, σ is the interaction cross section and $\alpha = (N_2 - N_1)\sigma$ denotes the frequency dependent absorption coefficient.

The gain G of the radiation after one pass (back and forth) through the active medium of length L is then

$$G(2L) = I(2L)/I(0) = \exp(-2\alpha L). \tag{7.08}$$

If R_1 and R_2 are the reflectivities, I is reduced by $R_1 \times R_2$ after one pass. Additionally, extra linear losses such as scattering and inhomogeneities, refraction and non-resonant absorption occur, which reduce the intensity after each pass by $\exp(-\gamma)$, such that the total becomes

$$G(2L) = I(2L)/I(0) = \exp(-2\alpha L - \gamma). \tag{7.08}$$

At the threshold value, the exponent must be zero, and we get for the second lasing condition

$$\Delta N = N_2 - N_1 > \Delta N_{\text{Threshold}} = \gamma/(2\sigma L). \tag{7.09}$$
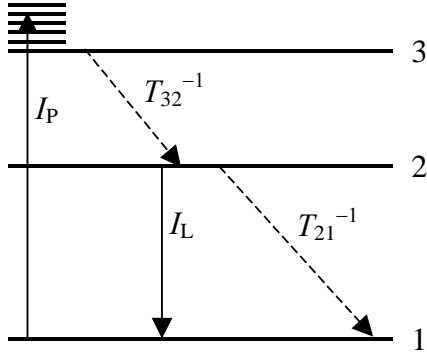
7.2.2   Optical Pumping

Fig. 7.9 Transitions in optical pumping using a three level laser (e.g. ruby laser). The lowest laser level 1 is the ground state of the system (electron ground state and/or vibrational ground state). The pump transition goes from level 1 to level 3 or a higher level from which the electrons can quickly get to level 3. Non-radiative transitions are shown as dashed arrows. T_{32} refers to the average lifetime of the electrons in level 3 until a transition to level 2 occurs. For this reason, T_{32}^{-1} is the transition rate.

The condition for effective pumping is $T_{32} \ll T_{21}$. We get with $P = \sigma_{13} I_P$ as pumping rate

$$N_3 \approx P\, T_{32}\, N_1 \ll N_1, N_2. \tag{7.10}$$

Further is

$$\frac{dN_2}{dt} = -\sigma_{12}\, I_L\left(N_2 - N_1\right) - \frac{N_2}{T_{21}} + P\, N_1 \tag{7.11}$$

and

$$\frac{dN_1}{dt} = +\sigma_{12}\, I_L\left(N_2 - N_1\right) + \frac{N_2}{T_{21}} - P\, N_1. \tag{7.12}$$

With $\Delta N = N_2 - N_1$ and $N = N_1 + N_2$ it follows that

$$\frac{d\Delta N}{dt} = -2\sigma_{12}\, I_L\, \Delta N - \left(P + \frac{1}{T_{21}}\right)\Delta N + \left(P - \frac{1}{T_{21}}\right)N. \tag{7.13}$$

In stationary conditions, $d\Delta N/dt = 0$ so

$$\Delta N_{\text{stationary}} = \frac{\left(P - \dfrac{1}{T_{21}}\right)N}{\left(P + \dfrac{1}{T_{21}}\right) + 2\sigma_{12}\, I_L}. \tag{7.14}$$

From the condition $\Delta N_{\text{stationary}} > 0$ it follows that

$$P_{\text{critical}} = \frac{1}{T_{21}}. \tag{7.15}$$

for the critical pump rate. Materials with a long relaxation time T_{21} are thus desired.

7.2.3 Optical Resonators

Analogous to the consideration of the modes in a cube with edge length L (see chapter 2.4) we get for a cuboid with a basal plane of $(2a)^2$ and length L where c is the phase speed of light in the medium under consideration

$$\boldsymbol{k} = \pi\,(n_x/2a,\ n_y/2a,\ n_z/L) \text{ and } \omega = c\,|\boldsymbol{k}| = c\,\pi\,\sqrt{\left(n_x/2a\right)^2 + \left(n_y/2a\right)^2 + \left(n_z/L\right)^2}\ . \quad (7.16)$$

We use only positive numbers for $n_{x,y,z}$ (see chapter 2.4). For rays close to the axis is

$$k_z \gg k_x,\ k_y \text{ and } n_z/L \gg n_x/2a,\ n_y/2a. \quad (7.17)$$

From that we can expand the root above:

$$\omega = c\,|\boldsymbol{k}| = \frac{2\pi\,c}{\lambda} \approx \frac{c\,\pi\,n_z}{L}\left(1 + \frac{L^2}{2(2a)^2}\frac{n_x^2 + n_y^2}{n_z^2}\right). \quad (7.18)$$

The electromagnetic field in the laser can be, in spite of the diffraction effects, described as supperposition of transverse electric and magnetic (TEM) modes, which have the three variable whole numbers n_x, n_y, n_z as indices. (In round rods, the values for x and y are replaced by polar coordinates.) For the frequency distance between two modes with $n_x = n_y = 0$, i.e. two neighboring principal modes with the longitudinal mode number q and $q+1$, TEM$_{0\,0\,q}$ and TEM$_{0\,0\,q+1}$ we have from $\omega = c\,\pi\,n_z/L$, compare to equ.(7.18),

$$\delta\omega_{\text{longitudinal}} = c\,\pi/L. \quad (7.19)$$

The separation between two neighboring transversal modes, in which only n_x (or n_y) differ by one, is according to equ.(7.18) and equ.(7.19)

$$\delta\omega_{\text{transvers}} = \delta\omega_{\text{longitudinal}}\,(n_x + \tfrac{1}{2})\frac{L\lambda}{8a^2} = \delta\omega_{\text{longitudinal}}\,\frac{n_x + \tfrac{1}{2}}{8N}, \quad (7.20)$$

where $N = a^2/(L\lambda)$ is the Fresnel number. In laser setups is $L \gg a$, and a several orders of magnitude larger than λ. The Fresnel number is therefore $N > 50$ and the frequency separation of two transvers modes is smaller than the separation of longitudinal modes.

The number N named after Augustin Fresnel determines the diffractive losses and can be understood through the following physical considerations: the blurring caused by diffraction of the angular aperture θ of a beam of wavelength λ at a pinhole diaphragm of diameter $2a$ is $\theta \approx \lambda/2a$, compare e. g. Demtröder: Experimentalphysik 2, Kapitel 10.5.1. With that, the relationship of the light coming through the diaphragm to that which does not get mirrored back into the diaphragm from a mirror a distance L away is

$$\pi\,a^2/[\pi(a + \theta L)^2 - \pi\,a^2] \approx a/(2\theta L) = a^2/\lambda L = N. \quad (7.21)$$

Let us now consider an ideal Fabry-Pérot-Resonator, in which no refractive losses occur due to the unhindered expansion of the two plane parallel mirrors Sp1 and Sp2. The reflectivity of the resonator is $R = \sqrt{R_1 R_2}$, where R_1 and R_2 are the reflectivities of the two mirrors. Correspondingly, $T = \sqrt{T_1 T_2}$ is the transmission of the resonator. The incoming and outgoing beams, as well as the exiting rays after single and double reflections are shown in Fig.7.10.
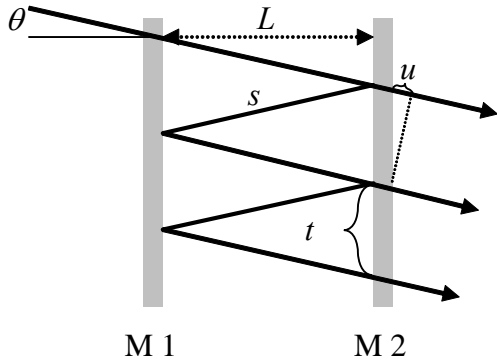

Fig. 7.10 A Fabry-Pérot-Resonator with a separation L between the mirrors, the angle θ between the incoming beam and normal to the mirror, the path length s when passing through the resonator, the shift t through back and forth travel, and the path length difference u between neighboring outgoing rays.

We get for the time average of the amplitude of the electric field E in relation to the incoming amplitude E_0

$$\frac{\overline{E}}{\overline{E}_0} = T\,\mathrm{e}^{\mathrm{i}\alpha}\left(1 + R\mathrm{e}^{\mathrm{i}\beta} + ... + R^n \mathrm{e}^{\mathrm{i}n\beta}\right) \xrightarrow{\;n\to\infty\;} \frac{T\,\mathrm{e}^{\mathrm{i}\alpha}}{1 - R\mathrm{e}^{\mathrm{i}\beta}} \tag{7.22}$$

behind the resonator after n double reflections and phase correct overlapping of the waves, ignoring the absorption and differing indices of refraction.

The phase differences

$$\alpha = \frac{2\pi}{\lambda}\,\frac{L}{\cos\theta} = 2\pi\frac{s}{\lambda} \quad \text{and} \quad \beta = \frac{2\pi}{\lambda}\,2L\cos\theta = 2\pi\frac{2s - u}{\lambda} \tag{7.23}$$

are explained as follows: the path s to be taken is longer than L, the phase shift with $2s - u$ is shorter than $2L$. It holds that $L/s = \cos\theta$, $t/2s = \sin\theta$, $u/t = \sin\theta$, $u = 2s\sin^2\theta$ and $2s - u = 2s(1 - \sin^2\theta) = 2s\cos^2\theta = 2L\cos\theta$. The intensity relationships correspond to the squares of the field strength or to the product of the field strengths with their conjugate complex quantities: $\overline{E}^2 = \left|\overline{E}\right|^2 = \overline{E}\,\overline{E}^*$. Using $1 - \cos\beta = 2\sin^2\beta/2$ we get for the total transmission T_{FP} of the Fabry-Pérot-Resonator

$$T_{\mathrm{FP}} = \left|\frac{\overline{E}}{\overline{E}_0}\right|^2 = \left(\frac{T}{1 - R}\right)^2 \frac{1}{1 + \dfrac{4R}{(1 - R)^2}\sin^2\dfrac{\beta}{2}}. \tag{7.24}$$

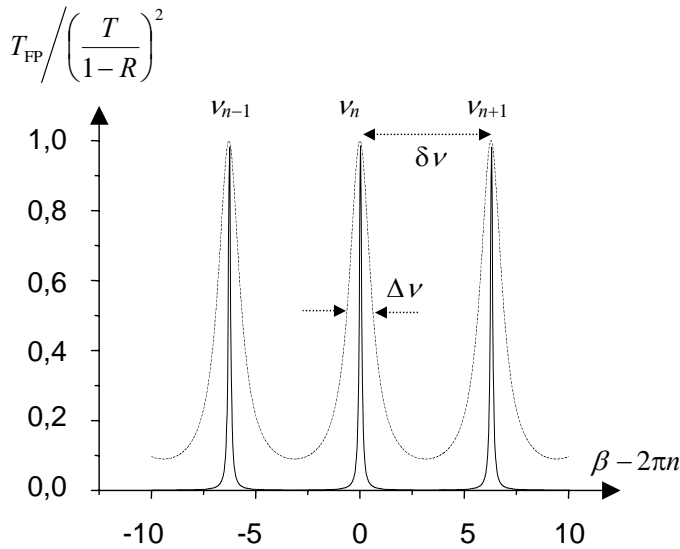$$T_{FP} \bigg/ \left(\frac{T}{1-R}\right)^2$$

Fig. 7.11 Transmission curve of a Fabry-Pérot-Interferometer for finesse coefficients 5 (dashed) and 50 (solid line). The wavelength range between subsequent maxima is the free spectral range $\delta\nu$, which amounts 2π. The corresponding β-range equals to $2L$ for perpendicular entrance ($\theta = 0$).
The corresponding frequency range in a vacuum is $c_0/2L$. In general we have $\nu_n = n\, c_0/(2L \cos\theta)$.

The FWHM in Fig. 7.11 referred to as $\Delta\nu$ can be determined on the β scale for $(1 - R) \ll R$ from equ.(7.24) and phase difference $\varepsilon = 2(1 - R)/\sqrt{R}$. A conversion into frequencies is done by division through 2π and multiplication with the frequency band $\delta\nu$:

$$\Delta\nu = \frac{2(1-R)}{\sqrt{R}}\frac{\delta\nu}{2\pi}. \tag{7.25}$$

By finesse, often labeled F^*, the relation of spectral range to FWHM is meant, see Fig. 7.11.

$$\frac{\delta\nu}{\Delta\nu} = \frac{\pi\sqrt{R}}{1-R}. \tag{7.25}$$

The finesse cofficient of the resonator is analogous to the quality factor of an oscillator in electronics. The advantages and disadvantages of a high quality factor are known in electronics: a high amplification in the frequency domain causes long die down times in the time domain.

In equ.(7.25), the finesse depends only on the reflectivity of the mirrors. In real systems, the surface roughness of the mirror and refractive losses from the non-infinite mirror diameter (finite Fresnel number) influence the finesse.

7.2.4 Descriptions of a few Lasers

The most important laser types can be classified according to their active materials into solid-state, gas, semiconductor, and dye lasers.

Nd-YAG solid-state lasers
Use Neodymium doped (1% of Yttrium positions) **Y**ttrium **A**luminum **G**arnet crystals, see the figure on the right, Fig. 14.25 from Meschede: Gerthsen-Physik, 22nd Edition.

Nd^{3+} (Z=60) has a larger radius than Y^{3+} (Z=39), therefore the doping is limited. Neodymium supplies one 4f electron and two 6s electrons, three 4f electrons are left over, the ground state of the Nd^{3+} ion is thus:

$$^4I_{9/2} \rightarrow J = L - S$$
$$L = 3+2+1 = 6$$
$$S = 3/2$$
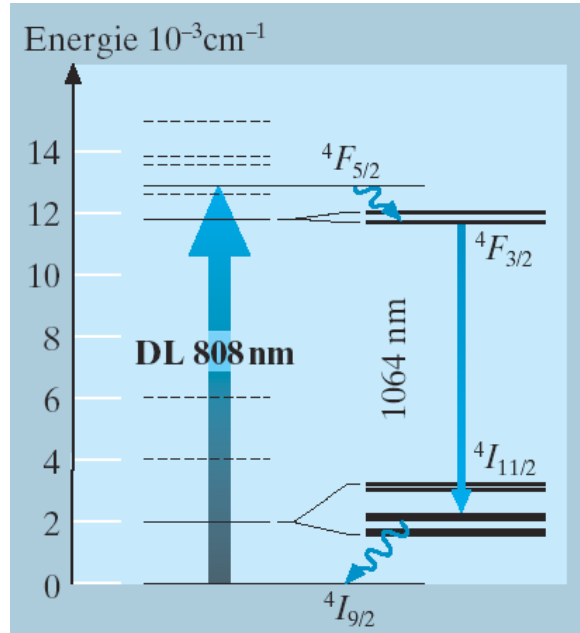
The crystal field splitting creates multiple $^4F_{3/2} \rightarrow {}^4I_{11/2}$ transitions, maximal fluorescence is at 1064 nm, frequency doubling delivers 532 nm, green light. The pumping used to be done with krypton lamps, now with high power laser diodes. The four-state laser has the advantage that much less than half of the electrons in the ground state are forced into the $^4F_{5/2}$-state, from which state they quickly relax into the $^4F_{3/2}$ level. In spite of the effective diode laser pump sources, the efficiency is less than 10% due to heat losses in the active medium.

Ruby laser
The world's first laser, a three-level laser, was built by Theodore Maiman in 1960. The historian laser uses ruby crystals, i.e. 0,1% Cr^{3+} at the locations of Al^{3+} in Al_2O_3. The three 3d electrons of Cr^{3+} are located at energy levels which are strongly affected by the crystal field (see chapter 5). The pumping level is a $^4F_2$ or $^4F_1$ level, the upper laser level is ^2E, the lower laser level is the same as the ground state $^4A_2$. The wavelength is 694 nm. A high pumping power is necessary, since for occupation inversion at least half of the Cr^{3+} ions from $^4A_2$ have to be moved into the ^2E state. The ruby rods are 0,2...2 cm thick and 2...20 cm long. They are generally operated as pulsed lasers with Xenon flash lamps. The efficiency is ≤ 1 %.

The emission from solid state lasers is characterized by a small coherence length (≤ 1 m) and poor homogeneity of the beam caused by spatial crystal inhomogeneities. A peaking effect (especially found in ruby lasers) occurs through the fast reduction of the occupation inversion for a mode which causes jumps between natural oscillations. From that, overlaps occur without periodicity, which statistically cause spikes with powers of up to 500 kW. (e.g. pumping pulse duration 5 ms, begin of lasing 0.5 ms after pulse start, spike duration 1 μs). Solid state lasers are generally found in non-linear optics, material processing, measurement technology (Lidar) and plasma production for nuclear fusion.

Helium neon lasers

Gas lasers are easy to cool by rapid flow through the cell. Helium and Neon are mixed about 5:1. Helium is excited and transfers its energy through collisions to metastable neon states, see figure at right, Fig. 8.9 from Demtröder: Experimentalphysik 3.

Argon lasers

Use 100% Argon. The excitation achieved through electron collisions in a discharge channel; Atom $\rightarrow$ Ionic ground state $\rightarrow$ pumping level. Because of L and J splitting of both laser levels, about 20 transitions from 450 to 530 nm can be used and selected with a prism in the laser tube. Efficiency 0,1%, well suited as pump source for dye lasers.

CO₂ lasers

Achieve the highest continuous output powers of some 10 kW with an efficiency of 10...20 %. In the gas discharge tube is CO_2, N_2, He and other gasses to prevent chemical reactions. The figure on the right is Fig. 8.30a from Demtröder: Experimentalphysik 3. The occupation of the upper laser level is achieved in the following way: In an electric discharge electrons excite a metastable N_2 level from which the energy goes to a CO_2 level by molecule collisions. The difference between the two excited levels is less than kT. The upper laser level is the first excited state of the antisymmetric valence oscillation of CO_2, the lower level is either the first excited oscillation state of the symmetric valence oscillation or the second excited state of the bending vibration (see chapter 3.3.3). Both are split through rotations. Correspondingly, the wavelengths are 10-11 µm or 9-10 µm, i.e. in mid IR. The resonators are one or more meters long and can be folded for large lengths.

Excimer lasers

refer to an excited diatomic molecule AB, *exci*ted di*mer*, which is only stable in an electronically excited state AB*. For this reason is the lower laser state poorly occupied and an inversion of the occupation through electron collision excitation from A and recombination with B is attainable: A*+B $\rightarrow$ AB*. Since the upper laser state is a well defined vibrational ground state of an excited electron level, but the lower an energy band of a certain width due to the rapidly (10^{-13} s) occurring decay AB $\rightarrow$ A + B + E_{kin}, the laser is limited tunable in the UV range. The energy rich radiation is used in medicine for cold ablation.
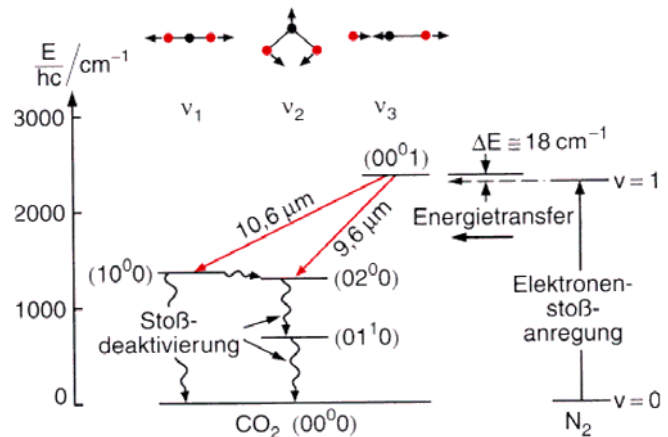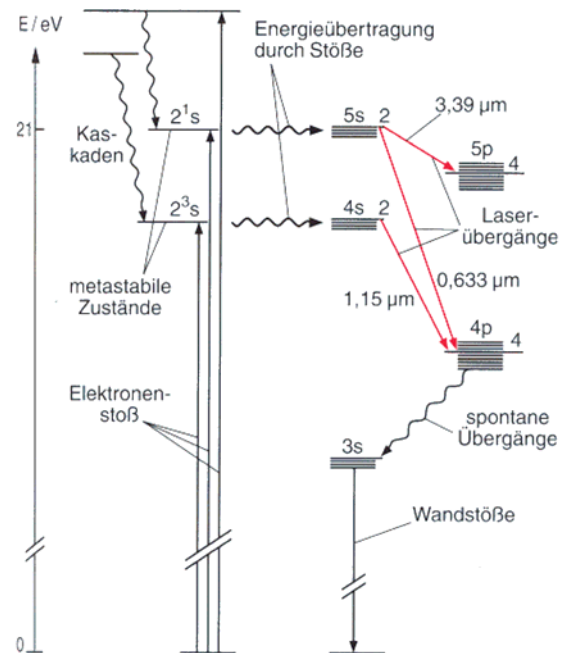
Semiconductor lasers
primarily use the occupation inversion created by carrier injection (diode in flow direction) of highly doped semiconductor diodes. The electrons from the conduction band of the n-doped material fall into the lower holes of the valence band of the p-doped material. The radiation emitted by the electron-hole recombination is amplified by passage through the p-n boundary layer so that for lengths of less than 1 mm the second lasing condition is fulfilled. The mirrors are often the untreated crystal boundaries. Luminescing transitions have a wavelength of 850 nm in a GaAs laser. Typical power ratings are around 10 mW. In diode arrays, 30 W output power and efficiencies of 25% have been achieved (albeit at the cost of beam quality). They are primarily useful as pumping lasers. The type of material (e.g. 4 components in InPGaAs) determine band gap and from that laser frequency as in LED's (*light emitting diodes*). The range of 400 nm to 4 µm is partially covered. A few types are tunable through variation of pressure, temperature, and current.

Dye-lasers
Make use of molecules of a fluorescent organic dye dissolved in a liquid as their active medium. The rotation-vibration splitting results in a relatively broad band for every electron level, in which the dye molecules quickly (10^{-10}–10^{-12} s) relax to the lowest vibration level from collisions with solvent molecules. Fluorescent transitions exist from the lowest S_1 state to all levels of the S_0 state. Since only the lowest vibration level of the deepest electron level is occupied in thermal equilibrium, the considerations for a four level laser are valid here. The lasers are pumped with a cw laser or flashlamps. Wavelength tuning is achieved with a grating, prism, or filter built into the beam path.
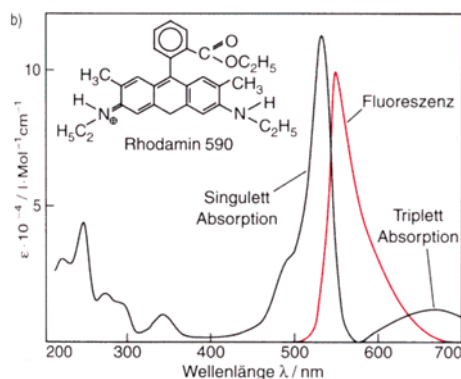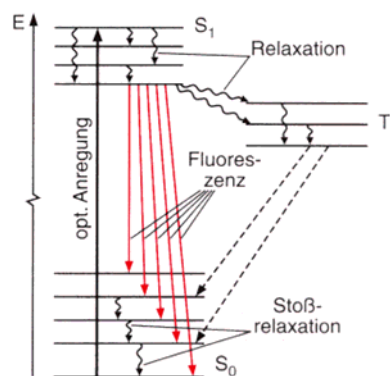
The existence of a triplet term system has proven to be disrupting, since the molecules stay in their ground state for a long time and are therefore not available for the lasing process (triplet quenching). This problem has to be solved by appropriate pulsed operation and/or a chemical quencher and/or pumping over into a freely flowing liquid jet (dye jet). The dye concentration is about 10^{-4} Mol L^{-1}, the solvent is ethanol, methanol or water. The dye molecule contains over 50 atoms, rhodamine 6G with molecular weight 479 is one of about 500 molecules.
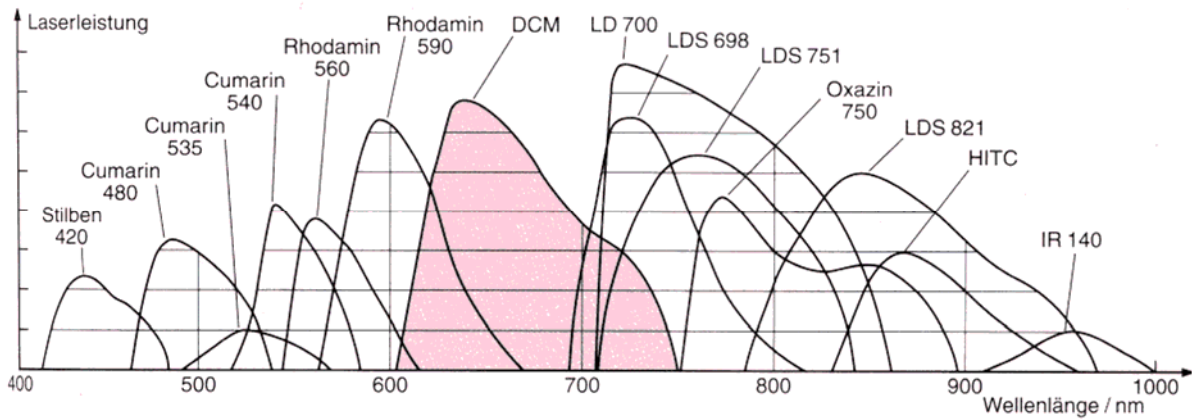
Dye lasers operate in the range of 300 to 1200 nm, where one type of dye covers around 50 nm. They are operated as cw lasers, flashlamp dye laser ($\approx 1\ \mu s$) and nanosecond dye lasers (5...20 ns). The first two types are pumped with cw gas lasers, the last type with N_2 or solid state lasers. Dye lasers are appropriate for spectroscopic investigations. The three figures above are Figs. 8.24ab and 25 from Demtröder: Experimentalphysik 3.

7.2.5   Producing Short Laser Pulses by Q-switching

Q-switching is done by artificially increasing the losses in the cell during the pumping pulse until a defined switching time t_s is reached. After this time, the laser losses return to their normal values.

When $t < t_s$, the laser cannot start to oscillate, because the oscillating condition is not fulfilled. At $t = t_s$ the threshold is reduced, and the beginning laser pulse rapidly destroys the population inversion. The Q-switcher is a Pockels cell, in which the crystal becomes double-refracting when a voltage is applied and the polarization plane of the transmitted light is rotated. An extra polarization beam splitter is added into the beam trajectory for the purpose of coupling out light in the normal (non-rotated) state; see the figure at right Figs. 8.32 and 8.33b from Demtröder: Experimentalphysik 3. Pulse lengths of a few nanoseconds can be achieved.
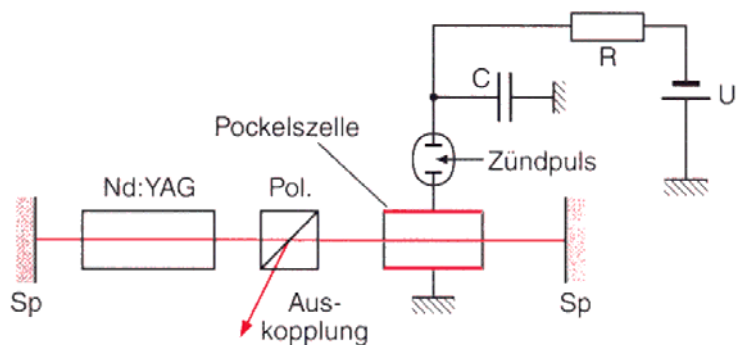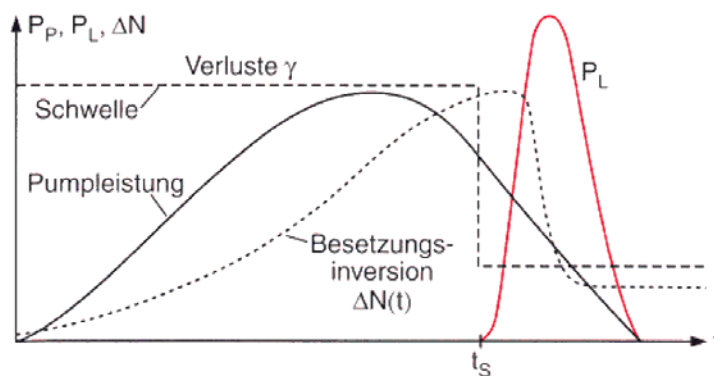
7.2.6   *Producing Ultra Short Pulses by Mode Locking*

In broadband laser transitions, many characteristic oscillations are produced. The total field strength of the laser radiation comes from the overlay of M axial characteristic oscillations:

$$E(t) = \text{Re} \sum_m E_m \exp\{i\varphi_m + i(\omega_0 + m\,\delta\omega)\,t\}, \qquad (7.26)$$

where the sum is from $m = -\frac{1}{2}(M-1), \ldots, \frac{1}{2}(M-1)$. The modal separation is $\delta\omega/2\pi = c/2L$, and E_m is the amplitude.

The phases φ_m can be statistically dependent or statistically independent. In the latter case we have white noise in the frequency interval in question, the so-called Gaussian noise. If,

Fig. 7.12 Gaussian Noise

however, a constant phase relationship can be determined between the various characteristic oscillations (mode synchronization, mode coupling, or mode locking), we get a periodic time dependency. If $E_m = E_0 = \text{constant}$ and $\varphi_m - \varphi_{m-1} = \alpha = \text{constant}$, φ_m can be replaced by $m\alpha + \varphi_0$ and the summation can be done analytically. We get
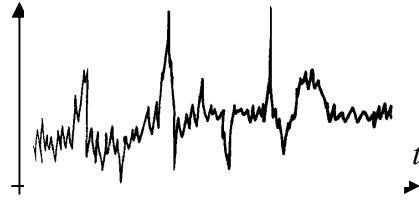
$$E(t) = E_0 \frac{\sin\left(M\dfrac{\delta\omega\,t+\alpha}{2}\right)}{\sin\dfrac{\delta\omega\,t+\alpha}{2}} \cos\omega_0 t + \varphi_0. \qquad (7.27)$$
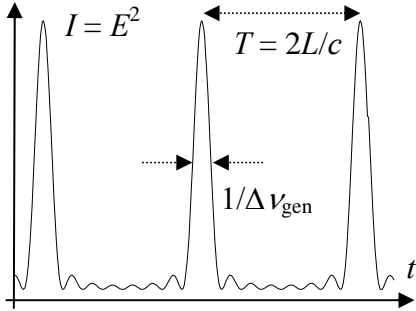

Fig. 7.13 Total intensity of the mode locked laser radiation from equ.(7.27) where $M = 8$.

For the distance between two neighboring maxima in Fig. 7.13 it holds that $T = 2\pi/\omega_0 = 2L/c$. The pulse length (fwhm) is $\tau = 1/\Delta\nu_{\text{gen}} = 2\pi/(M\,\delta\omega)$.

$\Delta\nu_{\text{gen}}$ refers to the frequency interval in which the modes die down. In heavy pumping, this corresponds to the line width of the laser transition. Increasing the line width of the laser transition or the number of modes for which the oscillation threshold has been crossed leads to a narrowing and increase in intensity of the pulses. For this reason, low pressure gas lasers are inappropriate for the production of short pulses. With solid state lasers about 1 ps is attainable, dye lasers achieve pulse lengths < 0.1 ps. The peak intensity for mode synchronized lasers is proportional to $M^2 E_0^2$. Without mode locking it is only proportional to $M E_0^2$.

The most common method for mode locking is *active mode synchronization* through periodic modulation of the resonator parameters. Laser losses (laser quality factor) and/or optical path lengths are modulated at a frequency by the action of a piezoelectric crystal on an optically transparent medium in the beam path of the cell, e.g. quartz. From that we get amplitude modulation of the laser frequency, where the modulation frequency is chosen so that it corresponds to the separation of the axial modes $2L/c$. This produces side bands of an oscillation that lie on neighboring modes and cause there neighboring oscillations that are synchronized with the principal oscillation.

7.2.7   Optical Pulse Compression

In chapter 2 we derived an index of refraction, equ.(2.17) from a linear relationship between electric field strength and polarization, equ.(2.15). The index of refraction depended on the frequency (dispersion) but not on the intensity of light. In the extremely high field strengths in lasers, the charge displacement is no longer linear to the field strength, and anharmonicities must be considered. Under consideration of the quadratic and cubic effects, the polarization of a particle becomes

$$P(E) = \mu + \alpha E + \beta E^2 + \gamma E^3, \tag{7.28}$$

where α, β and γ are tensors of second, third, and fourth rank. These non-linear optics (NLO) make frequency mixing possible, similar to electronic components with non-linear characteristic curves. This is the basis of some spectroscopic techniques that we will discuss later. Consideration of only the quadratic effect leads to an index of refraction that depends on the radiant intensity I

$$n(\omega, I) = n_0(\omega) + n_2 I. \tag{7.29}$$

The quadratic index of refraction can be either positive or negative, depending on the material. A laser beam with a radial Gauss shaped intensity profile experiences from this a lensing effect, which is used to focus the beam in the laser crystal. An aperture which only allows the central part of the light through can be inserted in the focal plane behind the crystal but still within the laser resonator. This has the effect of only allowing the pulse through around its maximum, since the lower intensities are stopped by the aperture. Pulse edges are stopped and the pulse is shortened. In the next pass, the pulse intensity is amplified, the focal plane is moved toward the mirror, and the aperture stops still more, etc.

In Titanium-Sapphire lasers where $\lambda = 700$ nm, a pulse width of 4 fs has been achieved, which is just 2 oscillation periods of the light. This method of the Kerr lens mode coupling (the Kerr effect is based on field strength dependent indices of refraction) is demonstrated in the figure to the right, Fig. 8.37 from Demtröder: Experimentalphysik 3.
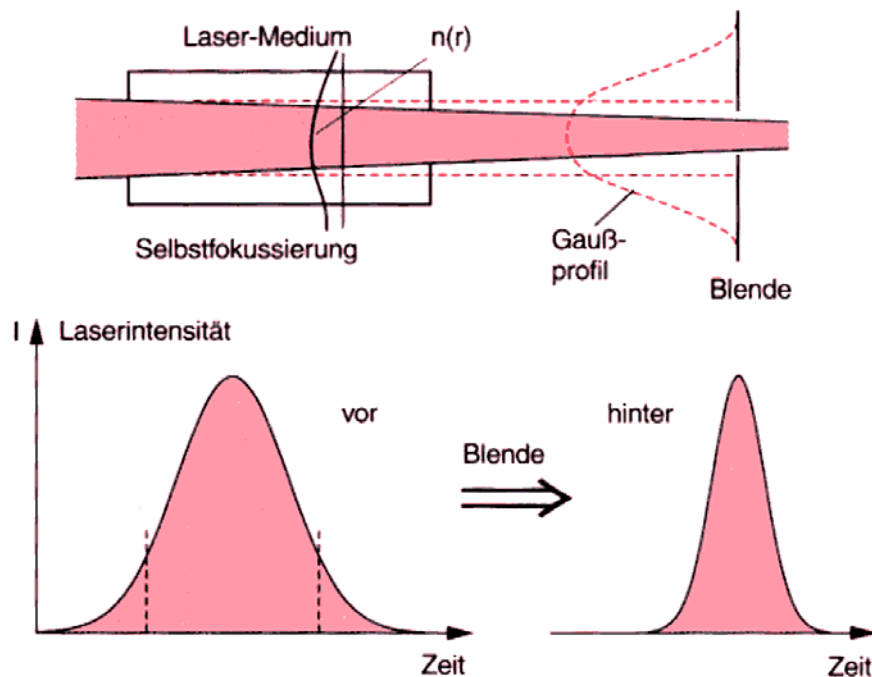
7.3   Time Resolved Laser Spectroscopy

Ultrafast spectroscopy allows us to observe rapid (femtosecond to nanosecond range) physical, chemical, and biological processes by mesuring the relevant physical parameters such as decay times of excitations. The observation of the dynamics of energy displacement, for example of an excited electron state on the vibration states or on the dissociation state, is hardly possible using other spectroscopic methods. Time resolved measurement processes are generally a two-step process. The first step is the excitation of the sample, the second is the measurement of the time dependent relaxation of the system. The excitation pulse is very powerful, a second can be weaker and from a different laser if common triggering from a pump laser can be guaranteed. From such a probe pulse at a different frequency, non fluorescent transitions can also be observed. The relaxation is specified by energy and charge transfer, diffusion processes, and reactions. The time dependency of the intensity of the fluorescent light, the spectral absorption or the index of refraction can be measured.

The experimental detection setup is set for the intensity of the radiation and the necessary time resolution. For fast photodiodes, time resolutions above 10 ps are possible. Photo multipliers (PM) have a poorer time resolution of 100 ps, but can measure single photons. If we are working with very high consequent frequencies in the megahertz range and very low pulse energies, such that the rate of the fluorescent events is small compared to the pulse rate, then single photon detection is appropriate. The laser pulse creates a starting pulse of the PM (or the photo detector, PD), which starts a time-to-pulse height converter (time linear increasing signal). The fluorescent photon causes a signal on a different PM which stops the converter and thereby creates a signal whose size is proportional to the time after the laser pulse. In the
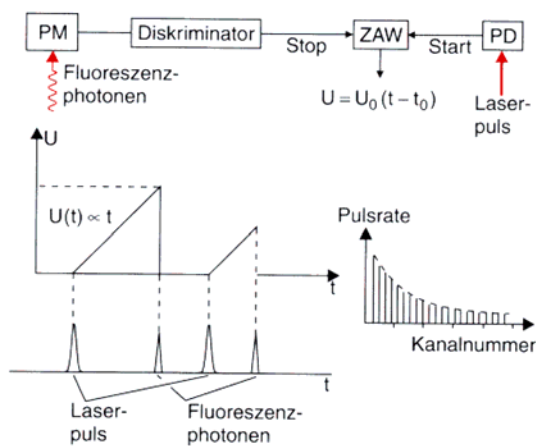
following pulse height discriminator, only a time resolution in the megahertz range is necessary so that a computer can determine the fluorescent events as a function of time. The picture to the left of the measurement of lifetimes with the help of single photon detection with delayed coincidence is Fig. 10.45 from Demtröder: Experimentalphysik 3.
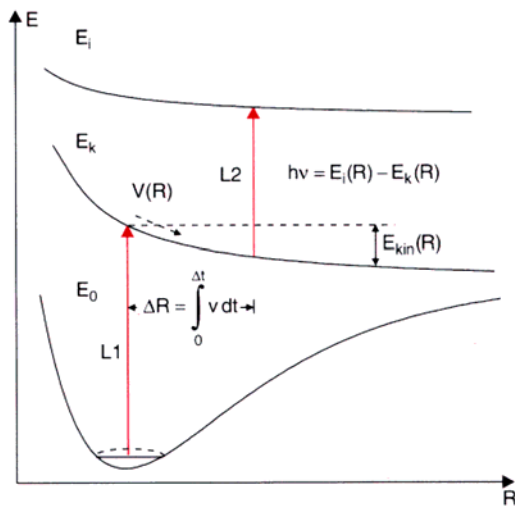
With the laser-induced fluorescence (LIF), *lifetime measurements* of fluorescent transitions of molecule A and its *deactivation cross section* for collision processes with molecule B can be determined. If we excite a special transition of molecule A with a relatively short pulse at time $t = 0$, we get the occupation N_0 in the upper state, which is not occupied in thermal equilibrium. This decays with the time constant τ_{eff}. The above setup makes such observations possible.

It holds: $N(t) = N_0 \exp{(-t/\tau_{\text{eff}})}$ where $\dfrac{1}{\tau_{\text{eff}}} = \dfrac{1}{\tau_{\text{spontaneous}}} + n_{\text{B}}\,\bar{v}_{\text{AB}}\,\sigma^{\text{inelastic}}.$ (7.30)

If τ_{eff} is measured as a function of the density of the collision partners n_{B}, the value for the average relative speed of the two collision partners $\bar{v}_{\text{AB}}$ can be calculated from the kinetic gas theory and contains the deactivation cross section for the collision process $\sigma^{\text{inelastic}}$ as well as the spontaneous lifetime $\tau_{\text{spontaneous}}$, which corresponds to the natural line width, by extrapolation to $n_{\text{B}} = 0$.

In the *pump and probe technique*, the sample is excited by a powerful pumping pulse. After an adjustable delay time, the occupation of the level is measured from the sample's absorption, amplification, reflection, or rotation of the polarization by means of a weak test pulse. The test pulse can have the same frequency as the excitation pulse or a frequency shifted, for example, in a Raman cell. With this method it is possible to trace the processes of photodisso-ciation of molecules, among others. We take advantage of the fact that the energies of two states i and k of one piece after the dissociation are functions of the distance R to the other piece. With that, also the difference $\Delta E = E_i(R) - E_k(R)$ is a function of R. The first powerful laser pulse lifts a particle vertically from the ground state of energy E_0 into the state k of energy E_k. A later probe pulse of energy $h\nu$ is only then absorbed, when the distance R has so changed in the time between the two pulses, that $\Delta E = E_i(R) - E_k(R) = h\nu$. With that, the time development of the dissociation is observable. The picture to the left is Fig. 10.49 from Demtröder: Experimental-physik 3.

7.4 Raman Spectroscopy with Lasers

Raman experiments were limited to a handful of substances with intensive signals before 1970, since the intensity of the non-resonant Raman scattering is 3-8 orders of magnitude below that of the resonance fluorescence of Rayleigh scattering. Through the use of lasers, a new renaissance of Raman spectroscopy began, since the increase in radiance of 10 orders of magnitude leads to a corresponding increase in sensitivity. A measurement setup is shown in Fig. 7.14, in which a grating double monochromator can be set to suppress the Rayleigh scattered radiation onto a set frequency when the dye laser is tuned.
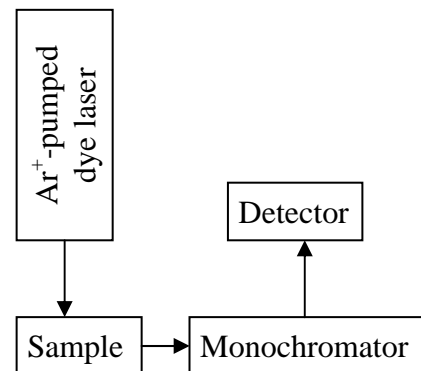
Fig. 7.14 *cw* Raman spectrometer

To increase the sensitivity, photon counting can be done with the detector, or the sample can be placed in the resonator of the laser. Resonant Raman scattering, in which the laser frequency corresponds to an excited electron level of the molecule, has better sensitivity. At 1 W laser power, between 10^{-9} and 10^{-10} W arrive at the radiation receiver. The limit of detection for the PM is about 10^{-16} W. This laser setup can be run continuously (continuous wave mode). Additional advantages gained through the use of lasers in the examination of biological substances include the avoidance of disturbing absorption of the sample through the choice of an appropriate wavelength of the laser and the examinability of small volumes. Raman laser microscopy is a proven method of spatially resolved material examinations.

Through the use of frequency mixing in non-linear optics, many new methods have been added to Raman spectroscopy. **CARS** stands for Coherent Anti-Stokes Raman Scattering, see Fig. 7.15. Two laser waves are input, ω_L, ω_S where $\omega_L > \omega_S = \omega_L - \omega_0$ and ω_0 is the oscillation frequency. A cubic process of four-wave mixing produces coherent radiation at the Anti-Stokes frequency $\omega_{aS} = \omega_L + \omega_0$, which is detected. The sensitivity of CARS is around 4 to 5 orders of magnitude above the linear (cs) Raman spectroscopy and can be further improved through resonant CARS (one or both virtual levels correspond to an excited electron level of the molecule).
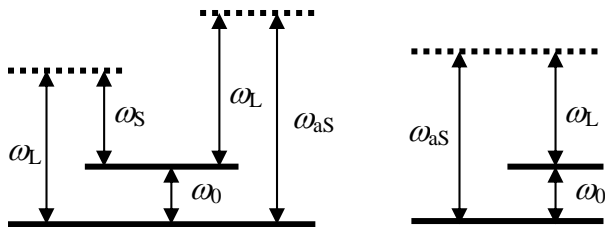

Fig. 7.15 Level diagram for CARS (left) and inverse Raman scattering (right). Dotted lines denote virtual levels.
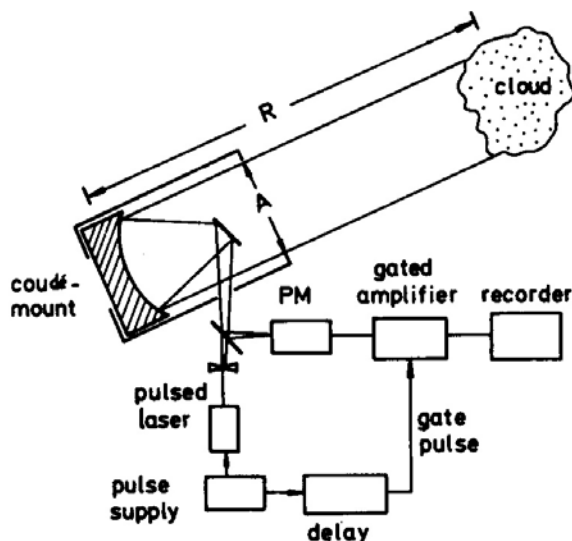
In **inverse Raman scattering**, the medium is illuminated by two lasers: ω_{aS} and $\omega_L = \omega_{aS} - \omega_0$, see Fig. 7.15. The absorption of ω_{aS} is observed. The disadvantage is the absorption measurement of the laser beam, advantage is the suppression of the fluorescent radiation. Inputting ω_{aS} in the form of broad band pulses can excite the complete Raman spectrum.

Raman Gain Spectroscopy uses an intensive laser wave ω_L and a weak probe wave $\omega_S = \omega_L - \omega_0$. The amplification of the Stokes frequency ω_S is measured.

7.5   LIDAR

LIDAR stands for *light detection and ranging* and is used for range dependent spectroscopy in the atmosphere to measure, for example, ozone concentrations. A short laser pulse with a wavelength at the absorption frequency of the substance in question is sent through a telescope at time $t = 0$ into the atmosphere. A part of the emitted light returns to the telescope due to Mie scattering on spherical dust and water droplets with dimensions on the order of the wavelength of the laser light, and from Rayleigh scattering on smaller particles,. With a gate circuit, the detector measures the backscattered light at the distance R after time t, which corresponds to a time $t = 2R/c$. The received power is a function of the absorption along the entire path, the solid angle, and the concentration and backscatter coefficient of the scattering particles. Only the first quantity depends (exponentially) on R. Alternating pulse frequencies are used. Although the first frequency is tuned to the observed absorption, the second is shifted to a value at which the molecule has no absorption, but the Mie scattering is not changed. The quotient is built from both values. Additionally, measurements are made at times t and $t + \Delta t$ and again the quotient of the results is built. This now only depends on the absorption between R and $R + \Delta R$. The picture to the left is Fig. 14.5 from Demtröder: Laser Spectroscopy.

.

7.6 Analogies between NLO and NMR

In coherent excitation of an optical transition with laser pulses of high field strength, which are shorter than its transversal relaxation time τ_{21} or longitudinal relaxation time $T_{21} = 1/k_{21}$, effects in optics which are similar to magnetic resonance spectroscopy can be observed. If the linearly polarized incoming field is in resonance, i.e. $\omega_L = \omega_{21}$, then a periodic occupation inversion is attainable, which depends on the pulse time τ and the so-called Rabi frequency

$$\omega_{\text{Rabi}} = \frac{1}{\hbar} M_{12} E_L . \tag{7.31}$$

M_{12} is the dipole moment of the transition, see equ (3.32), and E_L is the amplitude function of the laser beam. After the time $\omega_{\text{Rabi}}\, \tau = \pi$, an inversion of the occupation numbers occurs (π pulse). If we observe coherent collective decay from the excitation laser radiation after a $\pi/2$ pulse, we get, in analogy to magnetic resonance, free optic induction decay. This is inversely proportional to the inhomogeneous line width. A $\pi/2$, t, π pulse train causes a photon echo at time $2t$, whose decay is inversely proportional to the homogenous line width ($\delta\omega_{\text{hom}} = 2/\tau_{21}$). The time dependency of the echo amplitude is given by the transversal relaxation time τ_{21} or the relaxation factor $\{-2t/\tau_{21}\}$. With this experiment, homogenous and inhomogeneous line broadenings can be discerned from each other.

A 2π pulse rotates the macroscopic polarization amplitude by one complete rotation but does not change any occupation numbers and leaves no reason for relaxation processes. Such a pulse is not damped by travel through material. We speak of a self induced transparency. The pulse assumes a form which is not affected by further expansion. Such pulses are called fundamental solitons.

In chapter 4, in the description of the behavior of the macroscopic magnetization of nuclei disturbed from equilibrium by a high frequency field, the Bloch equations (4.29)

$$\frac{\text{d}\boldsymbol{M}}{\text{d}t} = \gamma \boldsymbol{B}_{\text{eff}} \times \boldsymbol{M} - \frac{M_x \boldsymbol{e}_x + M_y \boldsymbol{e}_y}{T_2} - \frac{\left(M_z - M_0\right)\boldsymbol{e}_z}{T_1} \tag{7.32}$$

appeared through the purely empirical input of relaxation terms into equ. (4.13)

$$\frac{\text{d}\boldsymbol{M}}{\text{d}t} = \gamma\, \boldsymbol{M} \times \boldsymbol{B} . \tag{7.33}$$

These Bloch equations were valid in the coordinate system rotating with the angular frequency $\omega_0 = \gamma B_0$, and the effective acting external field in this system is, see equ. (4.28),

$$\boldsymbol{B}_{\text{eff}} = (B_{\text{HF}},\, 0,\, B_0 - \omega/\gamma). \tag{7.34}$$

That was a short refresher before we handle the optical Bloch equations. For the definition of the other quantities used in the above three equations, see chapter 4.

In equ.(7.28), the polarization in the NLO with $P(E) = \mu + \alpha E + \beta E^2 + \gamma E^3 + ...$ was introduced, where α, β and γ are tensors of first, second, and third rank. A description of the non-linear interaction between light and material is no longer possible with this approach, if resonance effects appear. In that case, the system has to be described using coupled differential equations for electric and material fields. The corresponding NMR equation (7.32), which implicitly contains the excitation field strengths, was presented in 1946 by Ernst Bloch. In the optical Bloch equations no empirical approach is made, in contrast to NMR, but rather a derivation based on the density matrix will be presented.

We used the dipole moment of the transition introduced in chapter 3 in equ.(3.62)

$$M_{jk} = q \int \psi_j^* \hat{r} \psi_k \, d\tau , \qquad (7.35)$$

in an orthonormal basis defined with the Kronecker symbol δ_{jk}

$$\delta_{jk} = \int \psi_j^* \psi_k \, d\tau , \qquad (7.36)$$

where $\psi_{j,k}$ are the eigenfunctions of the unperturbed Schrödinger equation:

$$\mathcal{H}_0 \, \psi_j = \hbar \omega_j \, \psi_j \text{ where } j = 1,..., N. \qquad (7.37)$$

In general, the wave function is a linear combination of these states:

$$\psi(r,t) = \sum_{j=1}^{N} a_j(t) \psi_j(r) \qquad (7.38)$$

where, in the absence of polarization ($\mathcal{H} = \mathcal{H}_0$), it holds that

$$a_j(t) = a_j(0) \exp(-i\omega_j t). \qquad (7.39)$$

For a polarized atom we have in general

$$p_{\text{atom}} = e \int \psi^* \hat{r} \, \psi \, dr = \sum_{j,k} \rho_{jk} M_{jk} = Tr\{M\rho\} = P/n_a , \qquad (7.40)$$

where n_a is the number of atoms. The time dependent elements of the density matrix

$$\rho_{jk} = a_j a_k^* \qquad (7.41)$$

describe the solution of the unperturbed Hamiltonian, which is composed of $\mathcal{H}_0$ and the perturbation potential $\delta V = -e \, Er$. The field strength E should be constant over atomic distances.

For the calculation of the time dependency of the density matrix, we put equ.(7.38), with j replaced by ℓ, in the general Schrödinger equation

$$i\hbar \frac{\partial \psi}{\partial t} = \mathcal{H} \, \psi \qquad (7.42)$$

with $\mathcal{H} = \mathcal{H}_0 - eEr$, use equ.(7.37), j replaced with ℓ, multiply by ψ_j^* and we end up with equ.(7.35) and equ.(7.36)

$$\frac{\partial a_j}{\partial t} = -i\omega_j a_j + \frac{iE}{\hbar} \sum_{\ell=1}^{N} M_{j\ell} a_\ell \text{ where } j = 1,..., N. \qquad (7.43)$$

Equation (7.43) is multiplied by $a_k{*}$, then the complex conjugate of equ.(7.43) is calculated, j replaced with ℓ, and the result is multiplied by a_j and finally, considering that $p_{kt}{*} = p_{kt}$, everything is added. We get

$$\frac{\partial \rho_{ik}}{\partial t} = -i\left(\omega_j - \omega_k\right)\rho_{jk} + \frac{iE}{\hbar}\sum_{\ell=1}^{N}\left(M_{j\ell}\rho_{\ell k} - M_{\ell k}\rho_{j\ell}\right), \tag{7.44}$$

where j, k run from 1 to N, thus the impractical number of around N^2 equations appears. The relationship of the size of the second term to the first term on the right hand side of equ.(7.44) will be on the order of 10^{15} s^{-1} with the introduction of the transition frequencies $\omega_{jk} = \omega_j - \omega_k$, given by the relationship $E\,M_{jk}/\hbar\omega_{jk}$. We introduced the name Rabi frequency ω_{Rabi} for $E\,M/\hbar$, where $1/\omega_{\text{Rabi}}$ is a measure for the time in which the energy is transferred between the laser field and the atomic system.

The relationship $\omega_{\text{Rabi}}/\omega_{jk}$ lies between 10^{-4} and 10^{-7}. Nevertheless, we can not, in general, ignore the E terms in equ.(7.44). Even if the Fourier analysis of the perturbation terms shows only weak amplitudes at the transition frequencies ω_{jk} of the atoms, the density matrix is influenced proportionally with time:

$$\rho_{jk} - \rho_{jk}(0)\exp\left(-i\omega_{jk}t\right) \propto \frac{E\,M}{\hbar}t\exp\left(-i\omega_{jk}t\right). \tag{7.55}$$

This means that a cumulative resonance effect changes the density matrix.

These considerations are analogous to NMR: ω_{jk} corresponds to the Larmor frequency $\omega_L = \gamma B_0$, ω_{Rabi} to the nutation frequency $\omega_{\text{rf}} = \gamma B_{\text{rf}}$. In the transition to a *rotating* coordinate system, the time dependent effects only play a role when they also rotate. The effects are strongest when the rotations are *in* resonance.

In the consideration of the E terms, we can consider only those in resonance. The others can be described by an empirical relaxation term $-\gamma_{jk}\rho_{jk}$. (the γ used here has nothing to do with the gyromagnetic ratio of NMR.) With that we have only about n^2 equations (exactly: $n^2/2 + (n/2) - 1$), i.e. two equations for a two level system. The diagonal elements γ_{jj} correspond to irreversible losses, and the off-diagonal elements experience an extra contribution from elastic collisions. The damping described by γ is called homogenous broadening, in contrast to inhomogeneous broadening, see chapter 2.7.

The Bloch equations for transitions between n levels, which are in resonance with the incoming laser field, are thus

$$\frac{\partial \rho_{jk}}{\partial t} = -\left(\gamma_{jk} + \omega_{jk}\right)\rho_{jk} + \frac{iE}{\hbar}\sum_{\ell=1}^{n}\left(M_{jk}\rho_{\ell k} - M_{\ell k}\rho_{j\ell}\right). \tag{7.56}$$

Using the approaches for field strengths and polarization on the TEM$_{00}$ mode

$$E = A(t)\,V(r)\,\exp(-i\omega t) + A{*}(t)\,V{*}(r)\,\exp(i\omega t)$$

and
$$\tag{7.57}$$
$$P = \Lambda(t)\,V(r)\,\exp(-i\omega t) + \Lambda{*}(t)\,V{*}(r)\,\exp(i\omega t)$$

the amplitude functions $A(t)$ and $\Lambda(t)$ are defined, in which ω is the laser frequency. If we now only consider the dependency of the propagation direction z of a wave polarized in the x direction in a resonator with a homogenous medium, we can set $V(x, y, z) = \exp(i\omega z/c)$.

Nevell and Moloney (quoted at the end of this chapter) have shown that in this case, the relationship

$$\frac{\partial A}{\partial z} + \frac{1}{c}\frac{\partial A}{\partial t} + \frac{\kappa}{c}A - \frac{ic}{2\omega}\frac{\partial^2 A}{\partial x^2} = \frac{i\omega}{2\varepsilon_0 c}\Lambda \qquad (7.58)$$

for the amplitude of the resonator mode can be derived from the Maxwell equations. Here, however, a loss term has been artificially introduced, which describes the most significant losses that occur in laser cells by $\kappa = \dfrac{\sigma}{\varepsilon_0} + \dfrac{c}{L}\ln\dfrac{1}{\sqrt{R}}$.

To simplify our considerations, we will look at a 2 level gas. For the one dimensional wave, we have

$$\boldsymbol{P} = n_a\left(\boldsymbol{M}_{12}\rho_{12} + \boldsymbol{M}_{21}\rho_{21}\right) \qquad (7.59)$$

and

$$A(x,y,t) = A(x,y,t)\,\boldsymbol{e}_z , \qquad (7.60)$$

where $\boldsymbol{e}_z$ is the unit vector in the propagation direction z. For simplicity, we will also assume that $\boldsymbol{P}\|\boldsymbol{E}$ and $\boldsymbol{M}_{12}$ is real, thus $\boldsymbol{M}_{12} = \boldsymbol{M}_{21} = M\boldsymbol{e}_z$. From that it follows from equ.(7.57) and equ.(7.59) that

$$n_a M\rho_{12} = \Lambda(x,y,z,t)\exp\left(\frac{i\omega z}{c} - i\omega t\right), \qquad (7.61)$$

where Λ is in the propagation direction. According to definition, $\rho_{21} = \rho*_{12}$. From that we get the Block equations for ρ_{12} and $\rho_{22} - \rho_{11}$ with the assumption that $\gamma_{11} = \gamma_{22}$

$$\frac{\partial \rho_{12}}{\partial t} + \left(\gamma_{12} + i\omega_{12}\right)\rho_{12} = \frac{iEM}{\hbar}\left(\rho_{22} - \rho_{11}\right), \qquad (7.62)$$

$$\frac{\partial(\rho_{22} - \rho_{11})}{\partial t} + \gamma_{11}\left(\rho_{22} - \rho_{11}\right) = 2\frac{iEM}{\hbar}\left(\rho_{12} - \rho_{12}^*\right). \qquad (7.63)$$

If we set

$$N = n_a(\rho_{22} - \rho_{11}) \qquad (7.64)$$

and label the less energetic level with 2, then N is the difference in the occupation numbers, and becomes negative in the case of inversion. The pump rate necessary for stationary lasing $\gamma_{11}N_0$ is added to the right hand side of equ.(7.63). $EM(\rho_{12} - \rho_{12}*)$ is also replaced there by $1/n_a(A*\Lambda - A\Lambda*)$. With that, the $\exp(\pm 2i\omega t)$ terms which are not in resonance disappear. The result for the amplitude vector of the field strength, equ.(7.65)=equ.(7.58), is the polarization, equ.(7.66) from equ.(7.61) and equ.(7.62), and the difference in the occupation numbers, equ.(7.67) from equ.(7.63), and equ.(7.64), the Maxwell-Bloch equations.

$$\frac{\partial A}{\partial z} + \frac{1}{c}\frac{\partial A}{\partial t} + \frac{\kappa}{c}A - \frac{ic}{2\omega}\frac{\partial^2 A}{\partial x^2} = \frac{i\omega}{2\varepsilon_0 c}\Lambda , \qquad (7.65)$$

$$\frac{\partial \Lambda}{\partial t} + \left(\gamma_{12} + i(\omega_{12} - \omega)\right)\Lambda = \frac{ip^2}{\hbar}AN , \qquad (7.66)$$

$$\frac{\partial N}{\partial t} + \gamma_{11}(N - N_0) = \frac{2i}{\hbar}\left(A*\Lambda - A\Lambda*\right). \qquad (7.67)$$

The stationary solutions of the equations disregard the time dependencies of Λ and N

$$N = \frac{N_0}{1 + \dfrac{4M^2 A^2 \gamma_{12}}{\gamma_{11}\hbar^2\left(\gamma_{12}^2 + \left(\omega_{12} - \omega\right)^2\right)}} \, , \tag{7.68}$$

$$\Lambda = \frac{M^2 \dfrac{N_0}{\hbar}}{\gamma_{12}^2 + \left(\omega_{12} - \omega\right)^2 + \dfrac{4M^2 \gamma_{12}}{\hbar^2 \gamma_{11}} A^2} \left(\omega_{12} - \omega + \mathrm{i}\gamma_{12}\right) A \, . \tag{7.69}$$

Analogous to $\boldsymbol{P} = \varepsilon_0 \chi \boldsymbol{E}$, $\Lambda = \varepsilon_0 \chi\,(\omega,\, A^2)A$ can be thus described:

$$\chi\,(\omega,\, A^2) = \chi'\,(\omega, |A|^2) + \mathrm{i}\chi''\,(\omega,\, A^2)$$

$$= \frac{M^2 \dfrac{N_0}{\hbar\varepsilon_0}}{\gamma_{12}^2 + \left(\omega_{12} - \omega\right)^2 + \dfrac{4p^2 \gamma_{21}}{\hbar^2 \gamma_{11}} A^2} \left(\omega_{12} - \omega + \mathrm{i}\gamma_{12}\right) . \tag{7.70}$$

χ'' is the absorption signal and N_0 has to be sufficiently negative (occupation inversion), so that the medium acts as an amplifier. For low saturations of the medium, it holds that

$$\frac{4M^2}{\hbar}\frac{\gamma_{12}}{\gamma_{11}} A^2 \leq \gamma_{12}^2 + \left(\omega_{12} - \omega\right)^2 \tag{7.71}$$

and χ'' is a Lorentz line $(1/(1 + x^2)$, but χ' has the form $x/(1 + x^2)$ with respect to the variables.

Literature

Atkins, P., Physical Chemistry, 6th edition, Oxford University Press, Oxford, 1999
Demtröder, W.: Experimentalphysik 3, 2. Auflage, Springer, 2000
Demtröder, W.: Laser Spectroscopy, 3. Auflage, Springer, 2003
Meschede, D. (Ed.) Gerthsen Physik, 22. Aufl., Springer, 2003
Meschede, D., Optics, Light and Lasers, VCH, 2003, ISBN 3-527-40364-7
Newell, A.C., Moloney, J.V.: Nonlinear Optics, Addison-Wesley, 1992, 0-201-51014-6,
Pedrotti, F.L., Pedrotti, L.S.: Introduction to Optics, Prentice-Hall, 1993, 0-13-016973-0
Schrader, B. (Ed.).: Infrared and Raman Spectroscopy, VCH, 1995